JOURNAL OF AIRCRAFT
Vol. 45, No. 3, May–June 2008

# Determination of Wing-Only Aircraft Tumbling Characteristics Through Computational Fluid Dynamics

S. Saephan* and C. P. van Dam†
*University of California, Davis, Davis, California 95616*

DOI: 10.2514/1.33730

**Wing-only aircraft configurations are susceptible to a flight instability called tumbling. Tumbling involves an autorotative pitching motion, primarily about an axis parallel to the aircraft's lateral axis, combined with planar translation. Tumbling is the suspected cause of a wing-only aircraft (Northrop YB-49) crash in the late 1940s and is a potential problem for future wing-only and blended-wing–body aircraft configurations. It may be difficult, if not impossible, for a wing-only aircraft to escape the tumbling motion once it develops. It is therefore important for aircraft designers to understand the causes of tumbling to prevent its onset. Tumbling has been demonstrated in qualitative free-flight wind-tunnel experiments, but few have attempted to quantify the motion using computational fluid dynamics. The purpose of this research is to use computational fluid dynamics to study the tumbling characteristics of a wing-only aircraft. Specifically, the effects of initial conditions, degrees of freedom, Reynolds number, and aircraft static margin will be investigated.**

## Nomenclature

| | | |
|---|---|---|
| $C_D$ | = | aircraft drag coefficient |
| $C_L$ | = | aircraft lift coefficient |
| $C_m$ | = | aircraft pitching-moment coefficient about the center of gravity |
| $\bar{c}$ | = | mean chord length |
| c.g. | = | center of gravity |
| $I_{xx}$ | = | moment of inertia about the $x$ axis (roll axis) |
| $I_{yy}$ | = | moment of inertia about the $y$ axis (pitch axis) |
| $I_{zz}$ | = | moment of inertia about the $z$ axis (yaw axis) |
| $M_\infty$ | = | freestream Mach number |
| $q$ | = | pitch rate |
| $Re$ | = | Reynolds number based on the mean chord length |
| $V_\infty$ | = | freestream velocity |
| $\alpha$ | = | angle of attack |

## I. Introduction

TUMBLING is defined as the autorotative pitching motion, primarily about an axis parallel to the vehicle's lateral axis. It involves a three-degree-of-freedom (3DOF) motion in pitch and planar translation [1]. This mode of instability is inherent to wing-only aircraft. Experimental flying-wing or wing-only designs of the past include the propeller-driven Northrop XB-35 and its jet-powered derivative YB-49. More recently, aircraft manufacturers have been exploring tailless unmanned aerial vehicle configurations and the concept of a blended-wing–body (BWB) subsonic transport airplane. The BWB is appealing to aircraft manufacturers and their customers because of predicted performance improvements that include an estimated 15% reduction in takeoff weight and a 27% reduction in fuel burn per seat mile [2].

Maxwell [3] was one of the first researchers to attempt to explain the phenomenon of an autorotating card falling through air in the 1850s. For the next 100 years, not much attention was given to the tumbling phenomenon. In the 1940s, extensive tumbling tests were performed by Stone and Bryant [4] in the Langley 20-ft free-spinning tunnel. They investigated the tumbling characteristics of 14 dynamically scaled models by hand-launching the models into the vertical airstream. The ensuing motion was visually classified as *tumbled* or *no tumble*. In the 1990s, Fremaux et al. [1] experimentally investigated the effects of geometry and mass distribution on numerous tailless delta-wing models, including a generic model with a planform similar to the XB-35/YB-49.

Tumbling modes for flying wings are difficult to quantify. The onset of tumbling is highly sensitive to geometry, inertial properties, and initial conditions. Dynamic wind-tunnel tests to determine tumbling characteristics are very difficult to perform, and qualitative tumble/no-tumble results may be the only data available. High-speed cameras are sometimes used to photograph the model during testing to provide some indication of angular rates. The initial conditions for wind-tunnel tests can be difficult to quantify or repeat, especially if models are hand-launched into vertical airstreams.

More quantitative coefficients, such as stability and control derivatives, may be obtained from constrained 1DOF tests (free-to-pitch or forced-pitch oscillations), but tumbling is at least a 3DOF problem. The constrained testing procedures add uncertainty to the validity of the results. Also, dynamic wind-tunnel tests are typically conducted at Reynolds numbers that are at least several orders of magnitude smaller than full-scale flight Reynolds numbers. It is unclear as to how the lower Reynolds number test condition affects the results and whether the tumbling susceptibility is better or worse at full-scale flight conditions. Flight testing for these unconventional designs is hazardous, especially if the onset of tumbling is not known or not well understood. It is unclear if an aircraft can escape the tumbling motion once it begins. The flow becomes massively separated and control surfaces are likely to be ineffective. It becomes critical to know the causes and indications of tumbling to prevent its onset.

Computational fluid dynamics (CFD) has played a limited role in the field of aircraft stability and control [5]. It is often used to troubleshoot unforeseen problems after they occur. The attractiveness of CFD and today's primary reason for its use in the stability and control community is that it can provide a detailed description of the flow everywhere, something that is practically impossible to do in wind-tunnel or flight tests. CFD tools and computing resources are available to perform dynamic unsteady simulations of complete aircraft configurations at affordable cost with reasonable turnaround time. Tumbling characteristics are difficult to determine in wind tunnels and practically impossible in flight tests. CFD provides an appealing and viable alternative method to analyze the tumbling

Received 26 July 2007; revision received 30 October 2007; accepted for publication 4 November 2007. 

*Postdoctoral Researcher, Department of Mechanical and Aeronautical Engineering, One Shields Avenue; ssaephan@ucdavis.edu.

†Professor, Department of Mechanical and Aeronautical Engineering, One Shields Avenue; cpvandam@ucdavis.edu. Associate Fellow AIAA.

**Table 1 Properties of the YFW**

| | |
|---|---|
| Weight | 155,000 lb |
| $\bar{c}$ | 26.25 ft |
| Wing span | 172 ft |
| Wing area | 4020 ft$^2$ |
| $x_{\text{c.g.}}/\bar{c}$ | 0.275 |
| $z_{\text{c.g.}}/\bar{c}$ | −0.014 |
| $I_{xx}$ | $3.380 \times 10^6$ slug · ft$^2$ |
| $I_{yy}$ | $0.434 \times 10^6$ slug · ft$^2$ |
| $I_{zz}$ | $3.769 \times 10^6$ slug · ft$^2$ |

characteristics of aircraft. CFD can provide more than just a tumble/no-tumble answer. The simulation can provide detailed force and moment histories of the aircraft before and during the tumble. These force histories can be used to determine dynamic stability characteristics.

There was some renewed interest in studying tumbling when NASA and aircraft manufacturers began reexploring tailless aircraft configurations. This study uses CFD to investigate the tumbling characteristics of a generic tailless aircraft. Specifically, this study demonstrates that CFD can be used to simulate the onset and development of aircraft tumbling. Various simulations show the effects of degrees of freedom, Reynolds number, initial conditions, and aircraft static margin.

## II. Configuration

The geometry to be investigated is similar to the YB-49 and is designated as the YB-49-like flying wing (YFW). One particular test flight of the YB-49 out of then Muroc Air Force Base (AFB) crashed, killing all crew members onboard. Captain Glen Edwards was one of the copilots onboard. Muroc AFB was renamed Edwards AFB in his honor. The cause of the crash was never established, but it is suspected that the aircraft tumbled, because wreckage was found inverted, with little evidence of any horizontal velocity. The YB-49 program was eventually cancelled [6].

This configuration is chosen because the basic geometry is readily available. The mass, geometric, and inertial properties of the YFW are listed in Table 1. No flight-test data or wind-tunnel data are available, but dynamic tumbling data are not publicly available for any aircraft. Also, the fact that a YB-49 crashed, possibly due to tumbling, indicates that this aircraft configuration may be susceptible to tumbling.

A structured surface definition of the YFW is developed for CFD simulations. The simplified geometry is a single flying wing with no flaps, engines, or pylons, as depicted in Fig. 1. Each cross section is a NACA 65019. The NACA 65019 airfoil has a sharp trailing edge, but given the fact that zero-thickness trailing edges are not manufacturable, the trailing edge was made blunt for this study by truncating the airfoil at 98.5% of local chord.

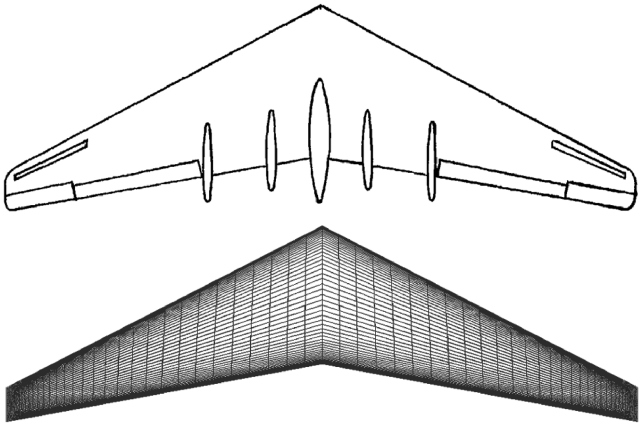

**Fig. 1 Surface grids for the YFW configuration.**

All grids are generated using Chimera Grid Tools [7]. The blunt trailing edge allows for the use of an O-grid topology and avoids a C-grid topology. The C-grid topology causes interpolation problems when the densely concentrated points in the wake region of the body-fitted grid traverse the much coarser background grids. The main wing grid has 600,000 points and each wingcap grid has an additional 200,000 points, for a total of 1,000,000 near-body points. The Cartesian offbody grids add an additional 500,000 grid points, for a grand total of 1,500,000 points. The normal grid spacing for the near-body grids have a $y^+$ value of approximately one.

## III. Computational Tools

The overset-grid flow solver (OVERFLOW2) is a three-dimensional Reynolds-averaged Navier–Stokes flow solver developed by Buning et al. [8,9] at NASA Langley Research Center, with support from many others. OVERFLOW2 requires overset structured Cartesian grids. Near-body volume grids containing the surface definitions are generated by the user. OVERFLOW2 can generate the offbody and far-field block Cartesian grids, cut holes using Meakin's x-ray methodology, and generate intergrid connectivity information [10,11].

Problems can be simulated as steady or unsteady, static or dynamic, and laminar or turbulent. OVERFLOW2 has several numerical schemes and most types of boundary conditions. Central difference is used for the right-hand side, along with an ARC3D diagonalized Beam–Warming scalar pentadiagonal scheme for the left-hand side. For time-accurate simulations, an implicit second-order-accurate Newton time-stepping scheme is used. The time-step size used in the simulations varies, but is no larger than an equivalent 0.02-deg change in angle of attack per step. Often, the time-step size is much smaller. At each time step, about five subiterations are performed to reduce the subiteration residuals by at least two orders of magnitude. OVERFLOW2 has five turbulence models, algebraic Baldwin–Lomax, one-equation Baldwin–Barth, one-equation Spalart–Allmaras, two-equation k-$\omega$, and two-equation Menter shear stress transport. For this study, the Spalart–Allmaras turbulence model [12] is used for all simulations.

Dynamic simulations can have either prescribed motion, general 6DOF motion, relative motion, or a combination thereof [13]. For prescribed motion, linear and angular velocities can be specified as functions of time. For general 6DOF simulations, rigid-body kinematics can be partially constrained (less than 6DOF) or completely unconstrained (6DOF). The body reacts to aerodynamic forces and moments and/or gravity. OVERFLOW2 is one of only a few flow solvers that can simulate dynamic motion.

OVERFLOW2 has been extensively validated for a wide range of stationary and moving-body aerodynamics problems. A previous investigation by the current authors used OVERFLOW2 to predict the forces and moments on forebody models with prescribed coning motion [14]. The predictions reasonably agreed with the experimental data, especially given the massively separated flow and dynamic conditions. Mayda et al. [15,16] studied the bubble-induced unsteady behavior of wind turbine airfoils and the effects of microtabs on airfoil aerodynamics. Potsdam and Strawn [17] used OVERFLOW2 extensively to study various helicopter configurations, including the tiltrotor V-22 Osprey. Chao and van Dam [18] applied the method to analyze the performance and loads of wind turbine rotors at attached and separated flow conditions. Buning et al. [19] performed computations on stage-separation problems of wing–body geometries at supersonic conditions. OVERFLOW2 was one of the flow solvers used in the Space Shuttle Columbia accident investigation [20–22]. These studies (along with numerous others not cited here, for which the computational results were obtained using OVERFLOW2 and validated with experimental data) demonstrate the capabilities of OVERFLOW2 and provide user confidence in the flow solver as a simulation tool.

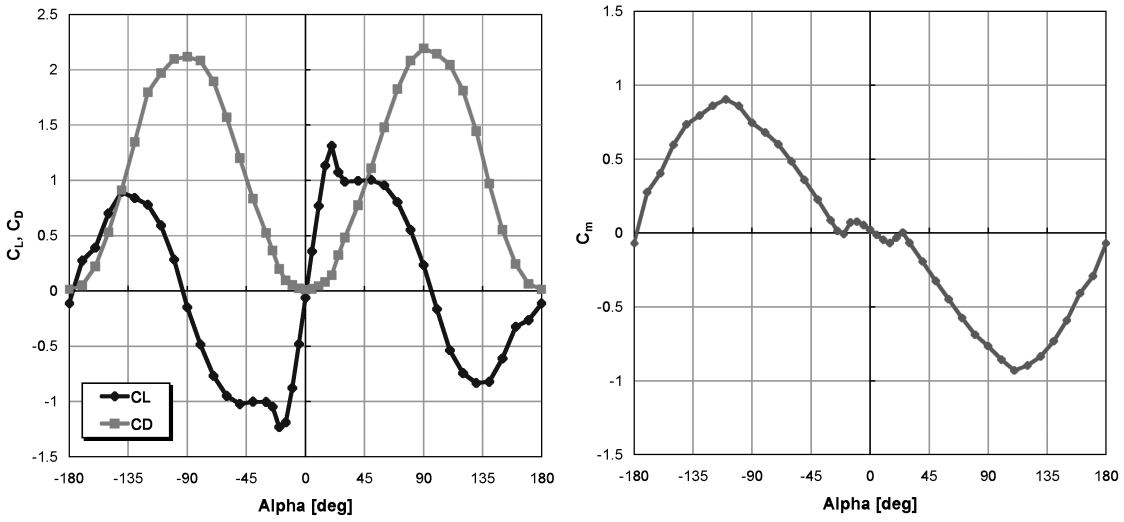


a) b)

**Fig. 2 Lift, drag (left), and pitching moment (right) coefficients for the YFW at static conditions.**

## IV. Results

### A. Simulation of YFW at Static Conditions

Aerodynamic coefficients for the YFW configuration were obtained for angles of attack from −180 to 180 deg under static conditions. Test conditions for these static simulations are $M_\infty = 0.15$ and $Re = 17 \times 10^6$. The flow is assumed to be fully turbulent. The lift, drag, and pitching-moment coefficients for the aircraft are shown in Fig. 2. For large angles of attack in which the flow is unsteady, the aerodynamic coefficients are averaged over several cycles.

The YFW has a small twist and dihedral, and so the lift curve is not symmetric and the drag curve is not symmetric between positive and negative angles of attack. For the particular angles computed, $C_{L_{\max}}$ occurred at $\alpha \simeq 20$ deg. The pitching moments are computed about the aircraft center of gravity, as specified in Table 1. The aerodynamic coefficients shown in Fig. 2 are only accurate for an aircraft under static conditions. Under dynamic motion, the coefficients are significantly altered due to dynamic effects. For simulations with motion, the measured $C_m$ values are the total $C_m$, which can be decomposed into a static contribution and a dynamic contribution. The static contribution is just the $C_m$ values at static conditions. The dynamic contribution is the difference between the total $C_m$ value measured at dynamic conditions and that measured at static conditions, as illustrated in Fig. 3.

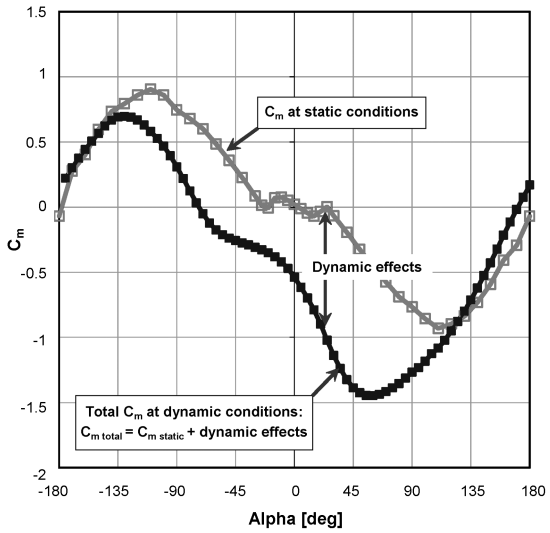


**Fig. 3 Static and dynamic contributions to the aircraft pitching moment.**

### B. Simulation of YFW at Prescribed Pitch Conditions

The YFW is prescribed to pitch for about one-and-a-half cycles (540 deg) at three different nondimensional pitch rates of 0.10, 0.22, and 0.40. The nondimensional pitch rate is defined as $q\bar{c}/2V_\infty$, with positive values indicating nose-up pitch. These rates are typical of advanced aircraft performing rapid maneuvers. The simulations are restarted from the $\alpha = 0$ deg steady-state solution. The initial transient effects from the solution restart decayed within the first 180 deg. The simulation results from the latter 360 deg are not affected by the initial transients.

The flow conditions for the prescribed pitch simulations are $M_\infty = 0.15$ and $Re = 17 \times 10^6$. Figure 4 shows the aircraft lift and drag coefficients as a function of angle of attack for pitch rates considered in the present study. At static conditions, the aircraft lift and drag are almost symmetric about $\alpha = 0$ deg, as already explained. Under the prescribed constant pitch rate, the dynamic effects cause the lift and drag to become very asymmetric about $\alpha = 0$ deg. Because the pitch is nose-up, the lift and drag for positive angles of attack are much larger than at negative angles of attack.

Even with the prescribed pitch motion, the lift at small angles is still linear with respect to angle of attack. The maximum lift coefficient increases with pitch rate. At the highest pitch rate of $q\bar{c}/2V_\infty = 0.40$, $C_{L_{\max}} \approx 4$, approximately three times larger than at static conditions. The maximum lift coefficient occurs around $\alpha = 45$ deg at the prescribed pitch conditions, compared with about $\alpha = 20$ deg for the static case.

Figure 5 shows the YFW pitching moment for the different prescribed pitch simulations. Within the linear lift regime ($-15$ deg $< \alpha < 15$ deg), the pitching-moment curve is nominally linear with a negative slope. The YFW indicates static longitudinal stability. As the aircraft pitch rate increases, the pitching-moment curves are shifted downward. The curves corresponding to higher pitch rates are shifted farther downward. Outside the linear lift regime, the pitching moment becomes highly nonlinear and dependent on the pitch rate and pitch direction.

### C. Effect of Degrees of Freedom and Initial Pitch Rates on Tumbling

Most dynamic wind-tunnel test techniques for longitudinal stability are usually limited to one degree of freedom, typically forced-oscillation or free-to-pitch tests. Although these tests are helpful and provide limited pitch-damping information, it is not known how representative these values are for a real aircraft with all six degrees of freedom. Tumbling is at least a three-degree-of-

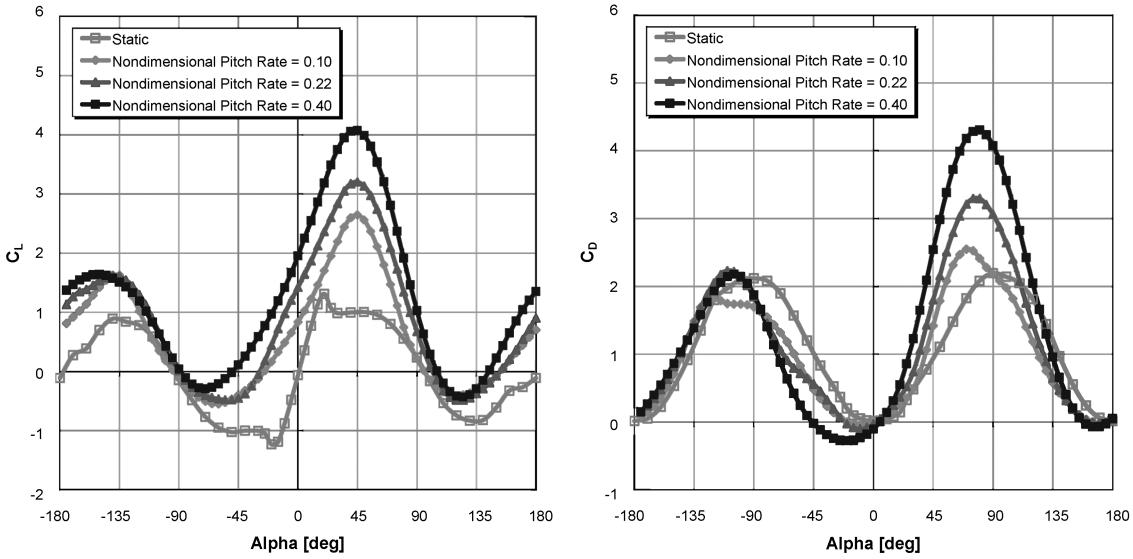


**Fig. 4 YFW lift (left) and drag (right) coefficients for the YFW during prescribed nose-up pitch at different pitch rates.**

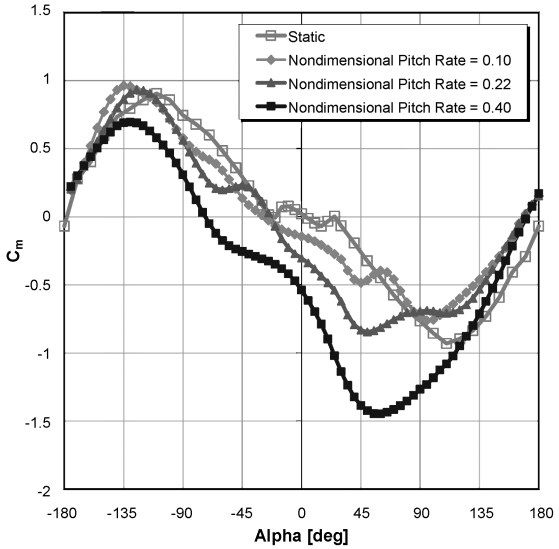


**Fig. 5 YFW pitching-moment coefficient during prescribed nose-up pitch at different pitch rates.**

freedom problem, in which the translational degrees of freedom may play a significant role in the tumbling instability, either to sustain or damp the motion. Any sideslip angle or aircraft spanwise asymmetries will cause the 3DOF tumbling motion to evolve into a full 6DOF motion. One objective of this study is to compare tumbling susceptibility in 1DOF and 6DOF.

Static longitudinal stability is the tendency of the aircraft to develop a pitching moment that opposes a disturbance in angle of attack from its steady-state flight condition. For static longitudinal stability, the aircraft center of gravity needs to be forward of its aerodynamic center. The pitching moment as a function of angle of attack needs to have a negative slope. Having positive static longitudinal stability is important, but does not by itself guarantee dynamic longitudinal stability. Dynamic longitudinal stability is the tendency of the amplitudes of the motion of the aircraft, following a disturbance in angle of attack, to decrease to zero. Static and dynamic longitudinal stability characteristics for the YFW can be ascertained from simulation results.

A series of test conditions were simulated to quantify the difference between 1DOF motion and 6DOF motion. The flow conditions are $M_\infty = 0.15$ and $Re = 17 \times 10^6$ and are assumed to be fully turbulent. These flow conditions apply to all cases, unless otherwise noted. Each simulation is conducted in three phases. The first phase is to simulate the aircraft at static conditions at zero angle of attack. The next phase involves a nose-up pitch motion about the center of gravity that is prescribed at some constant pitch rate until the aircraft reaches $\alpha \approx 50$ deg. Note that the 50-deg release point is arbitrarily chosen. At the 50-deg release point, the simulation is switched from the prescribed nose-up pitch motion to either a 1DOF or 6DOF motion. The dynamic response of the aircraft is simulated for several flight seconds, long enough to see if the initial pitch motion will lead to a tumbling motion or will damp out. The aircraft forces and moments, angular and translational velocities, angular orientation, and spatial position are recorded throughout the simulation for later postprocessing. The duration of each simulation depends on the aircraft behavior and may be different between simulations.

Three initial pitch rates are simulated: $q\bar{c}/2V_\infty = 0.20$, 0.22, and 0.40. Angular rate coefficients of these magnitudes are more typical of high-performance aircraft, but certainly still plausible for flying-wing configurations. The different test cases will be referred to by these pitch-rate initial conditions.

The 1DOF and 6DOF responses in terms of geometric angle of attack and corresponding pitch rate are shown in Fig. 6. For this case, with an initial pitch rate of $q\bar{c}/2V_\infty = 0.20$, both 1DOF and 6DOF responses are similar in the sense that the aircraft continues its nose-up pitch, begins to invert itself after passing the 90-deg angle of attack, but the nose-up pitch damps out before the aircraft reaches the 180-deg angular orientation and transitions to a nose-down pitch toward $\alpha = 0$ deg. The aircraft overcorrects and enters negative angles of attack. The last few seconds of the simulation show that the aircraft's nose-down pitch eventually damps out and the aircraft is once again correcting toward $\alpha = 0$ deg. In both cases, the aircraft does not enter a tumbling mode. In fact, Fig. 6 indicates that the aircraft is in a damped-oscillation mode. Note that these simulations do not model any stability and control augmentation system.

Figure 7 shows the aircraft pitching moment during the 1DOF and 6DOF simulations, as a function of both time and angle of attack. The significant difference between the 1DOF and 6DOF responses is apparent. A negatively sloped $C_m$-vs-$\alpha$ curve indicates a positive static longitudinal stability that tends to restore the aircraft back toward equilibrium. However, a positive $C_m$-vs-$\alpha$ slope indicates an unstable condition that is further propelling the aircraft away from equilibrium. Figure 7 shows regions with positive and negative longitudinal stability. The effect of hysteresis on $C_m$ is apparent in Fig. 7 when $C_m$ values are plotted as a function of angle of attack. The

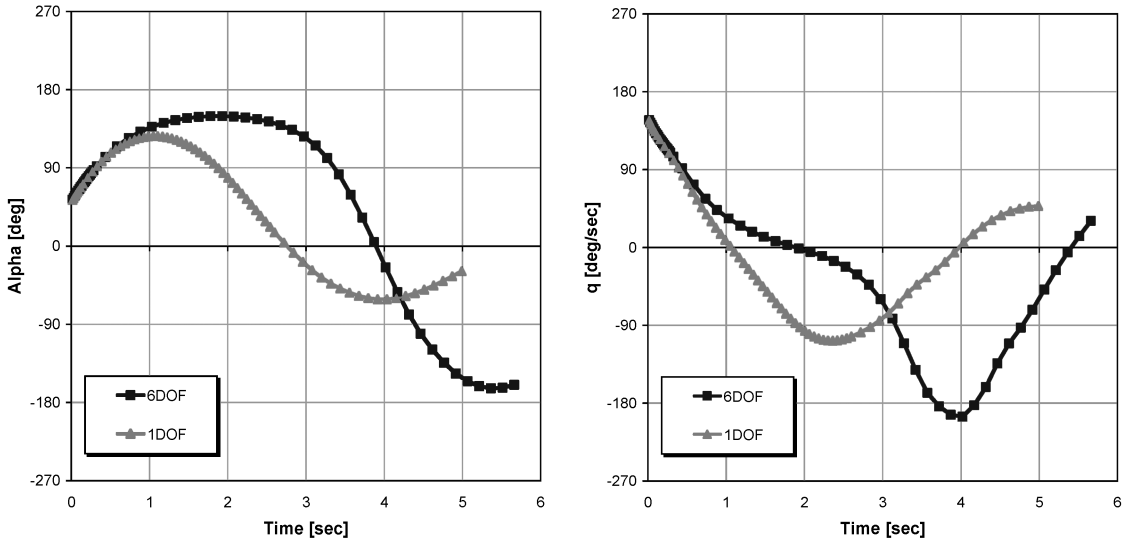


a) b)

**Fig. 6 YFW orientation and (left) pitch rates (right) as a function of time for the 1DOF and 6DOF simulations after an initial $q\bar{c}/2V_\infty = 0.20$ nose-up prescribed pitch.**

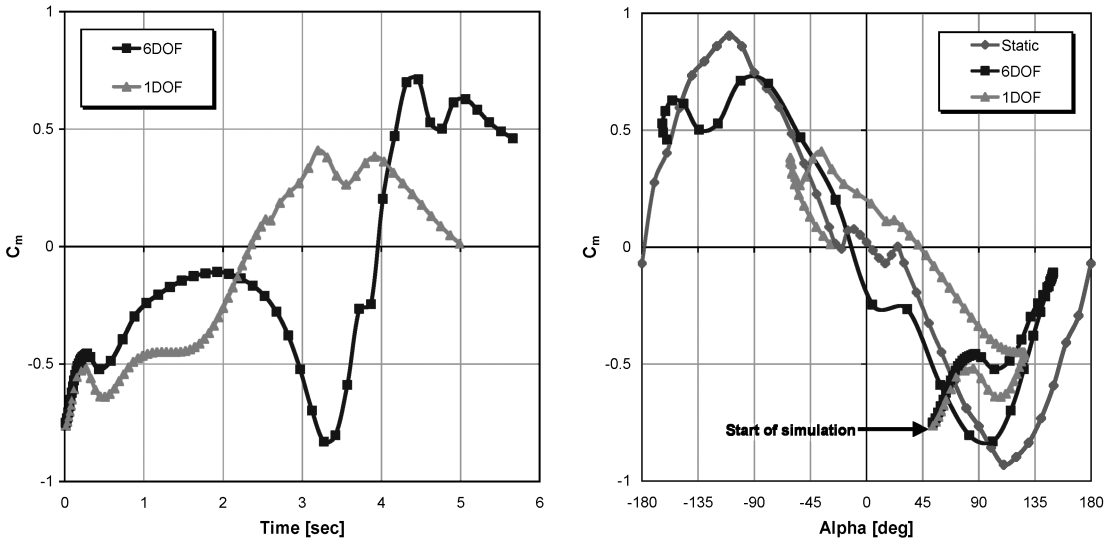


a) b)

**Fig. 7 $C_m$ as a function of time (left) and $C_m$ as a function of angle of attack (right) for the 1DOF and 6DOF simulations after an initial $q\bar{c}/2V_\infty = 0.20$ nose-up prescribed pitch.**

YFW exhibits one function of $C_m$ for a nose-up pitch and another function of $C_m$ for the nose-down pitch.

Figure 8 depicts the aircraft angle of attack and pitch rate as a function of time for the case with an initial nose-up pitch of $q\bar{c}/2V_\infty = 0.22$. For this case, the 1DOF simulation indicates a no-tumble motion by the fact that the nose-up pitch is damped out before the aircraft reaches a fully inverted orientation of 180 deg and transitions to a nose-down motion. Whereas the 1DOF simulation did not tumble, the 6DOF case indicates a possible tumbling instability, because the aircraft has pitched at least one full cycle. However, the nose-up pitch motion appears to damp out on the second pitch cycle. Figure 9 depicts the aircraft $C_m$ during the 1DOF and 6DOF simulations. Again, there is a significant difference between the 1DOF and 6DOF results.

Figure 10 illustrates the aircraft angle of attack and pitch rate as a function of time for the case with an initial nose-up pitch of $q\bar{c}/2V_\infty = 0.40$. Both the 1DOF and 6DOF simulations indicate an initial tumbling instability. The 1DOF case underwent a complete 360-deg pitch cycle and the 6DOF case underwent two complete cycles. The average pitch rate for the second tumble cycle is less than the initial cycle, indicating that the tumbling motion may eventually damp out. During the first two seconds of the simulation, Figs. 10 and 11 show similar behavior for the 1DOF and 6DOF cases. This is a strong indication that the angular momentum from the initial nose-up pitch is dominant over all other effects in the initial moments. Because the 6DOF case underwent two pitch cycles, the dynamic $C_m$ values plotted as a function of angle of attack clearly show regions of resisting and propelling pitch. The region of resisting pitch (negative $C_m$ for nose-up pitch) is larger than the region with propelling pitch (positive $C_m$ for continued nose-up pitch through negative angles of attack), indicating that the tumbling motion is not self-sustaining and will damp out.

### D. Effect of Aircraft Static Margin on Tumbling

All the preceding cases are for a YFW configuration with 8% static margin. The effect of aircraft static margin on the susceptibility and sustainability of tumbling is investigated by simulating a YFW configuration with 1% static margin. Although the static margin is small, the configuration is still considered stable as long as the static

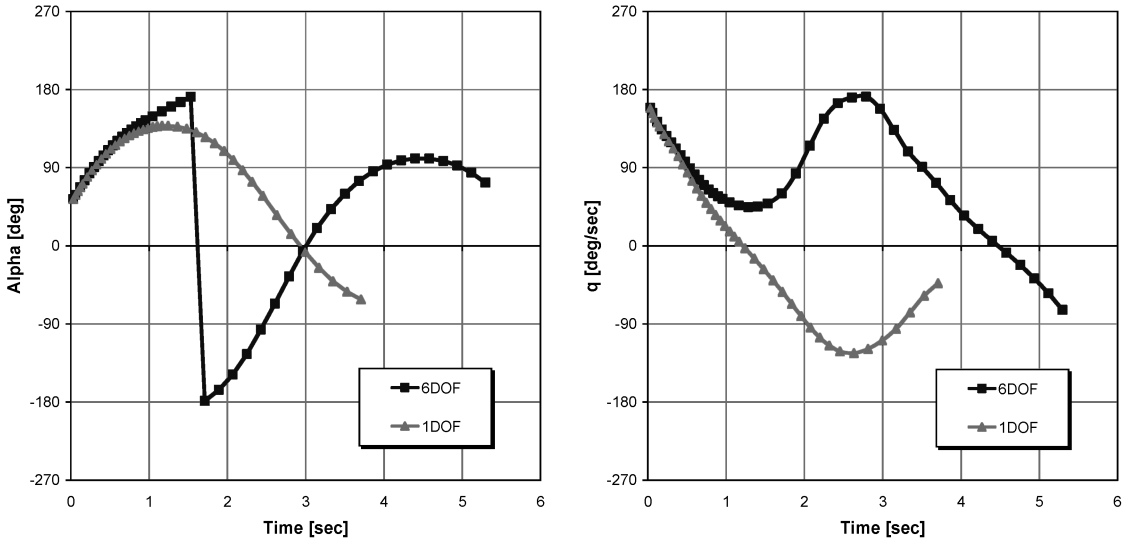


a) b)

**Fig. 8 YFW orientation (left) and pitch rates (right) as a function of time for the 1DOF and 6DOF simulations after an initial $q\bar{c}/2V_\infty = 0.22$ nose-up prescribed pitch.**

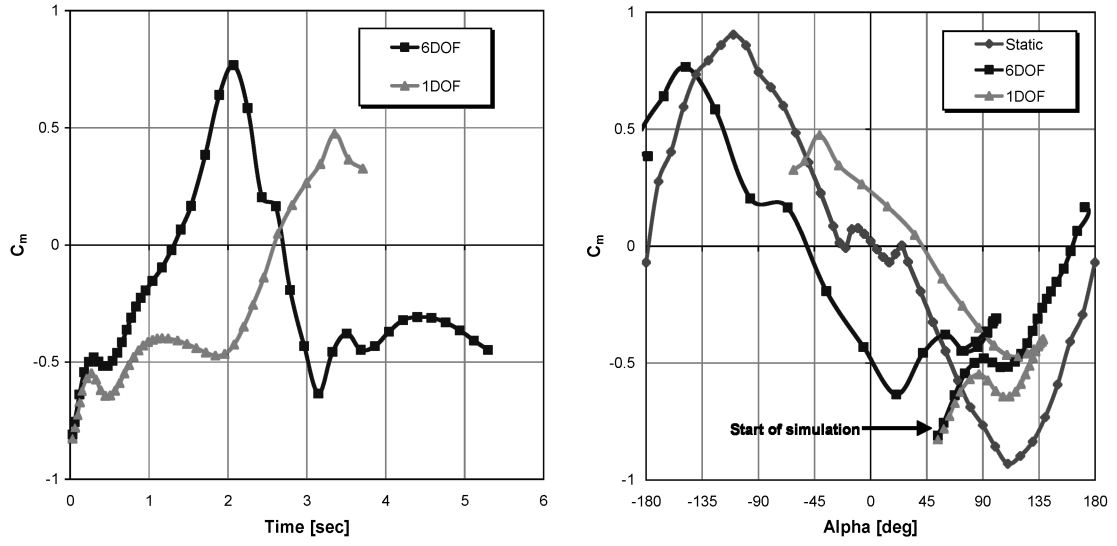


a) b)

**Fig. 9 $C_m$ as a function of time (left) and as a function of angle of attack (right) for the 1DOF and 6DOF simulations after an initial $q\bar{c}/2V_\infty = 0.22$ nose-up prescribed pitch.**

margin is positive. The 6DOF response for the 1% static margin case is compared against the 8% static margin case in Fig. 12. These simulations were conducted after an initial prescribed $q\bar{c}/2V_\infty = 0.22$ nose-up pitch.

Whereas the 8% static margin configuration tumbled for one cycle and then started to damp out, the 1% static margin configuration appears undamped. In fact, the average pitch rate seems to be increasing, unlike the decreasing trends observed in all the 8% static margin configurations. The aircraft's pitching moment, as depicted in Fig. 13, shows that the region of resisting pitching moment covers about a 180-deg range, followed by a region of propelling pitching moment of approximately the same range. This would help sustain the tumbling motion.

Figure 14 depicts the trajectory of the YFW center of gravity and its angular orientation. Clearly, the YFW is tumbling. Although the simulation allows for movement in all six degrees of freedom, the tumbling is confined to just 3DOF, with 1DOF in pitch and 2DOF in planar translation. Note that the YFW configuration is spanwise symmetric, the freestream velocity vector is parallel to the aircraft longitudinal axis, and the initial prescribed moment is about the pitching axis only.

There are no quantitative data available for tumbling experiments; hence, it is difficult to directly compare the computational results with measured data. However, Fremaux et al. [1] did perform some qualitative tumble/no-tumble tests on a number of dynamically scaled models in the 1990s. In Fig. 15, there are two points representing wind-tunnel tests for the XB-35/YB-49. For one test case with about 10% static margin, the model did not tumble. However, for a model with about 1% static margin, the model did tumble. A similar trend is observed in this investigation. A simulation in which the YFW has an 8% static margin did not tumble (Fig. 8), but another simulation with just 1% static margin and all else the same (Fig. 12) did tumble, effectively repeating the tumble/no-tumble trend observed in the vertical-spin tunnel and providing some qualitative validation to the numerical results. These results clearly indicates that the amount of static margin has a significant effect on the susceptibility and sustainability of tumbling for the YFW.

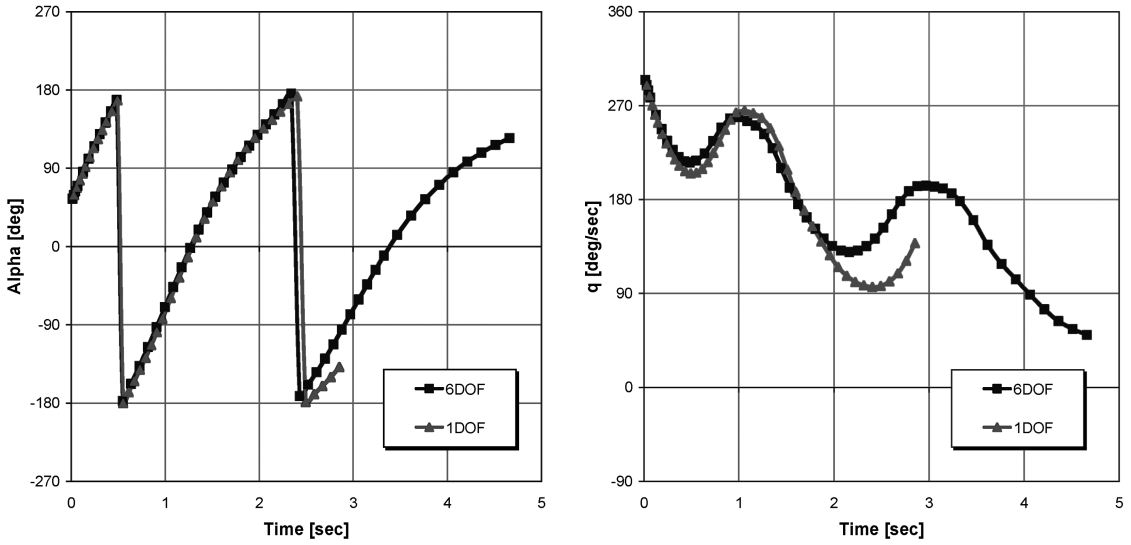


a) b)

**Fig. 10 YFW orientation (left) and pitch rates (right) as a function of time for the 1DOF and 6DOF simulations after an initial $q\bar{c}/2V_\infty = 0.40$ nose-up prescribed pitch.**

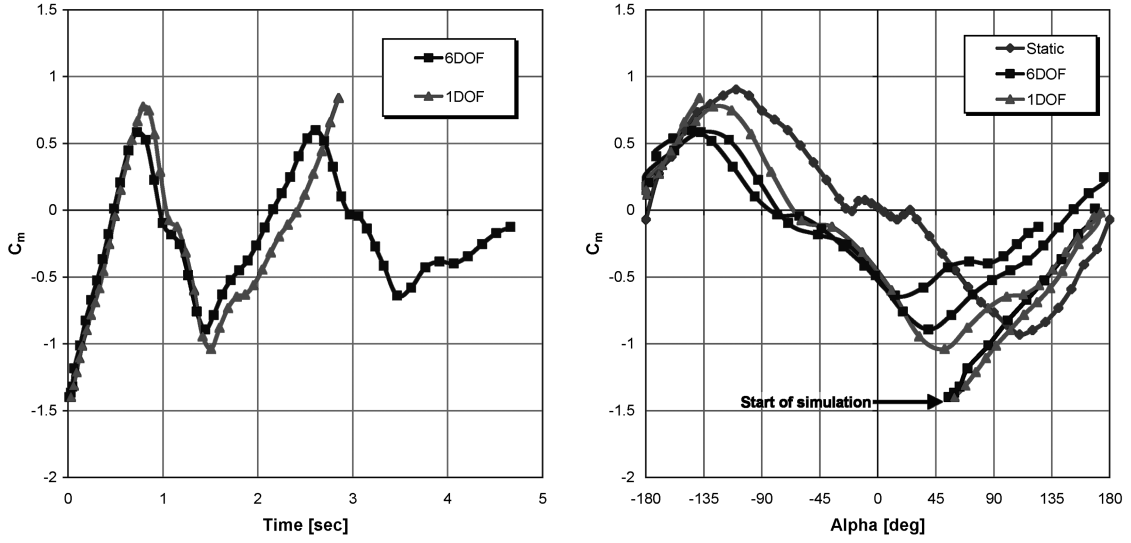


a) b)

**Fig. 11 $C_m$ as a function of time for the 1DOF and 6DOF simulations after an initial $q\bar{c}/2V_\infty = 0.40$ nose-up prescribed pitch.**

### E. Effect of Reynolds Number on Tumbling

Wind-tunnel experiments of scaled models are often conducted at Reynolds numbers much lower than a flight Reynolds number. This adds uncertainty to the test data when extrapolated to the flight Reynolds number. Several cases were simulated at different Reynolds numbers to determine the effect of Reynolds number on the tumbling phenomenon.

The results previously presented are simulated as fully turbulent at $Re = 17 \times 10^6$. Additional cases are simulated as fully laminar at $Re = 0.1 \times 10^6$, about two orders of magnitude lower than before and within the ballpark of Reynolds number conditions in wind tunnels. All other initial and boundary conditions are kept the same between the simulations. The initial nose-up pitch rate is $q\bar{c}/2V_\infty = 0.22$. Figure 16 shows the effect of Reynolds number on tumbling. Even though there were two orders of magnitude difference between the two Reynolds number conditions, the change in dynamic response is not dramatic. The 6DOF laminar case showed that the YFW tumbled one cycle, whereas the 1DOF laminar case did not indicate a tumble at all, essentially repeating the trend observed at the $Re = 17 \times 10^6$ condition. In fact, the results indicate that the $Re = 0.1 \times 10^6$ condition is slightly less damped than the $Re = 17 \times 10^6$ condition.

## V. Discussion

To ensure that the computational results are grid-independent, a grid convergence study is conducted. The baseline grid used throughout this study has approximately 1.5 million points, with about 1 million points in the near-body grids and the remaining points in the offbody Cartesian grids.

A coarser grid with about 0.88 million points and a finer grid with about 2.7 million points, roughly half of and double the baseline grid, respectively, are used for the convergence study. The grids are used to simulate steady static conditions at $\alpha = 0$, 5, and $-10$ deg; $M_\infty = 0.15$; and $Re = 17 \times 10^6$ based on the mean aerodynamic chord. Coefficients of lift, drag, and pitching moment are compared in Table 2. The side force, rolling moment, and yawing are essentially zero for this spanwise symmetric configuration.

Results obtained on the coarse mesh indicate that the grid density is insufficient. Changes in the magnitude of lift and drag were both

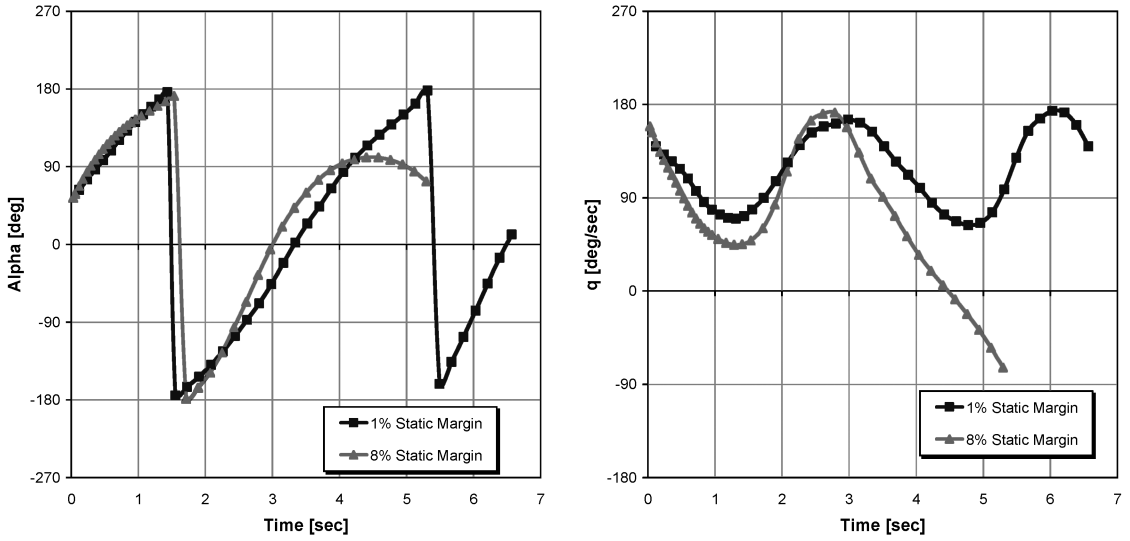


a) b)

**Fig. 12 YFW orientation (left) and pitch rate (right) for 6DOF simulations with 1 and 8% aircraft static margins.**

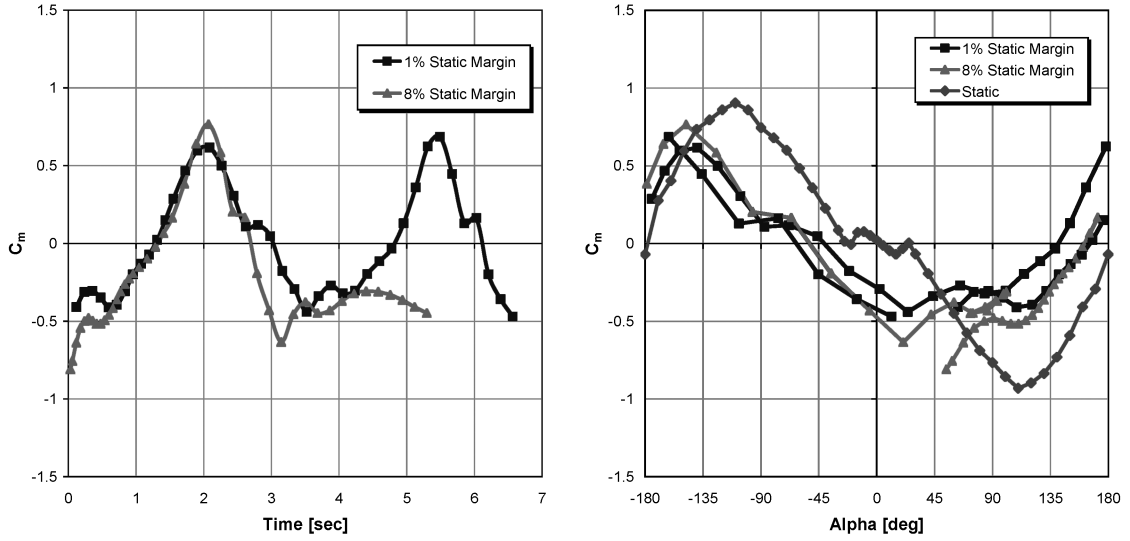


a) b)

**Fig. 13 YFW pitching moment as function of time (left) and function of angle of attack (right) for 6DOF simulations with 1 and 8% aircraft static margins.**

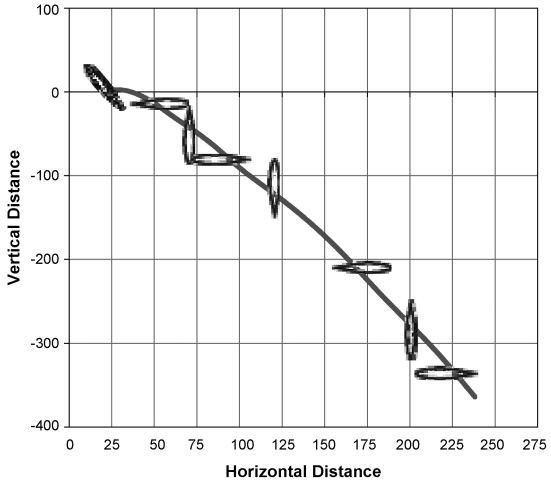


**Fig. 14 Location of center of gravity and angular orientation of the YFW during a 6DOF simulation with 1% static margin.**

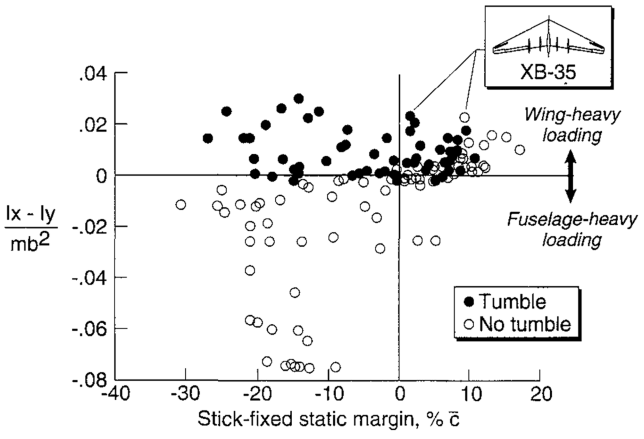


**Fig. 15 Experimental results for 12 flying-wing models at various mass loadings. Reprinted from Fig. 4 of [1]. XB-35 data points were originally plotted by Fremaux using data from [4].**

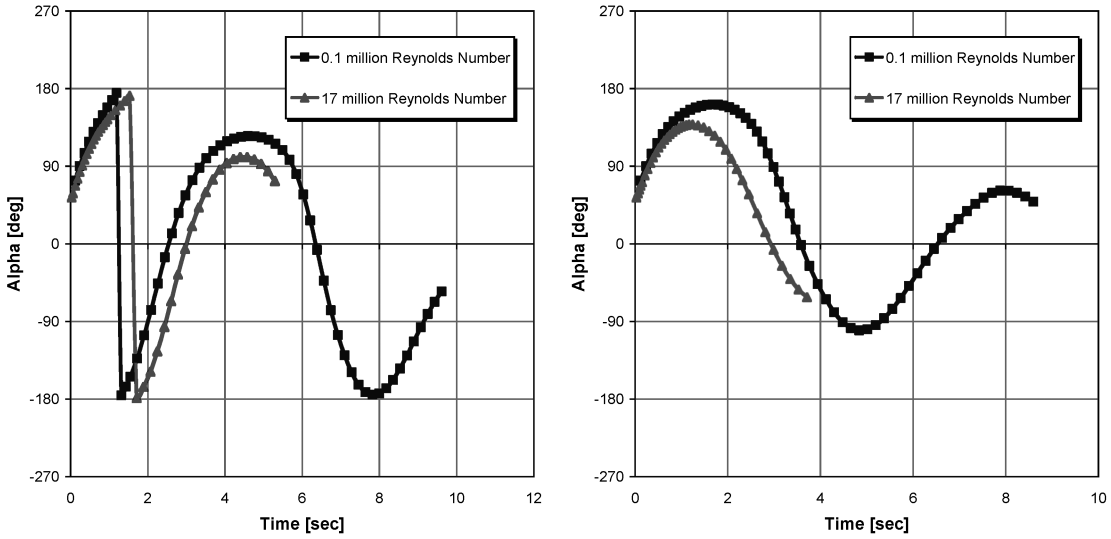


**Fig. 16 Aircraft orientation for a 6DOF (left) and 1DOF (right) simulation as a function of time for simulations conducted at different Reynolds numbers.**

less than 5%, but the change in pitching moment is significant, as high as 35% at $\alpha = 5$ deg. Simulations performed on the fine grid indicate that the baseline grid is sufficient. In all three angle-of-attack cases, the differences in lift were 1% or less. The differences in drag were consistently 6% and the differences in pitching moment were 3% or less for all three angle-of-attack cases. Given that the pitching moment plays a critical role in the tumbling motion, yet remains little changed between the baseline- and fine-grid simulations, it is reasonable to assume that the baseline grid has sufficient resolution to capture the flow physics. Even though the grid convergence study is conducted at small angle-of-attack conditions, the conclusion can be extended to large angle-of-attack conditions. As long as the near-body grids have sufficient resolution to capture the flow physics near the surface, OVERFLOW2's grid-adaptation routines automatically and regularly adapt offbody grids based on body movement and solution error.

The results show that the tumbling problem has a significant dependence on initial conditions and aircraft static margin. Depending on the initial pitch rate, the pitching motion will continue until either the aircraft tumbles or the motion damps out. The simulations show that the aircraft pitching motion can damp out and the pitching moment attempts to restore the aircraft to an equilibrium condition, even when the aircraft angle of attack is well past stall.

The various simulations clearly demonstrate that there is a difference between a constrained 1DOF problem and an unconstrained 6DOF problem. The dynamic response of the aircraft to an initial nose-up pitch differs, with the 6DOF scenario being less damped and more prone to tumbling. This can be partially explained through a total energy perspective. Assuming comparable losses for both 1DOF and 6DOF cases, the sum of potential energy, kinetic energy (for linear velocities), and rotational energy (for angular velocities) should remain the same between the 1DOF and 6DOF simulations. When the aircraft descends in 6DOF mode, it is losing some of its potential energy. Although some of that loss is dissipated as heat, some of it is converted into kinetic and rotational energy, thereby making the 6DOF case more prone to tumbling. For the same initial and boundary conditions, the 1DOF results are not conservative. A case was shown in which the aircraft did not tumble in 1DOF, but did indeed tumble in 6DOF. In all directly comparable 1DOF and 6DOF cases, the 6DOF motion is less damped. This observation should be taken into account when using 1DOF experimental data to predict 6DOF tumbling instabilities.

**Table 2 Aerodynamic coefficients for YFW at static conditions**

| | | Baseline grid | Coarse grid | Fine grid |
|---|---|---|---|---|
| $\alpha = 0$ deg | $C_L$ | −0.0640 | −0.0603 | −0.0646 |
| | $C_D$ | 0.0111 | 0.0112 | 0.0105 |
| | $C_m$ | 0.0210 | 0.0192 | 0.0211 |
| $\alpha = 5$ deg | $C_L$ | 0.3570 | 0.3450 | 0.3583 |
| | $C_D$ | 0.0173 | 0.0170 | 0.0161 |
| | $C_m$ | −0.0135 | −0.0086 | −0.0132 |
| $\alpha = -10$ deg | $C_L$ | −0.8788 | −0.8371 | −0.8883 |
| | $C_D$ | 0.0513 | 0.0495 | 0.0482 |
| | $C_m$ | 0.0768 | 0.0618 | 0.0788 |

The 6DOF simulations show that both the tumbling and nontumbling responses remain confined to three degrees of freedom, with one degree of freedom in pitch and two degrees of freedom in planar translation. For this investigation, the YFW configuration is spanwise symmetric, the freestream velocity vector is parallel to the aircraft longitudinal axis, and the initial prescribed moment is about the pitching axis only. In the real world, it is unlikely that the aircraft will be spanwise symmetric and initial perturbations will most likely include flow sideslip along with rolling and yawing moments.

## VI. Conclusions

Wing-only aircraft are susceptible to tumbling. Determining the cause and onset of tumbling is difficult. Qualitative tests only indicate tumbled or no tumble, whereas quantitative tests are often constrained to 1DOF and are performed at low Reynolds number. The only viable method to evaluate this mode of instability is through computational fluid dynamics simulations. For this study, a YB-49-like flying-wing configuration (YFW) is simulated to investigate its tumbling characteristics. The effects of initial condition, degrees of freedom, Reynolds number, and aircraft static margin are investigated. Various simulations show that the YFW is more susceptible to tumbling in 6DOF than in 1DOF and at low Reynolds numbers than at high Reynolds numbers. Initial conditions such a prescribed nose-up pitch strongly affect and can initially dominate the aircraft's dynamic response. Limited aircraft static margin can increase the susceptibility to tumbling and sustain the tumbling motion once it begins.

## References

[1] Fremaux, C. M., Vairo, D. M., and Whipple, R. D., "Effect of Geometry and Mass Distribution on Tumbling Characteristics of Flying Wings," *Journal of Aircraft*, Vol. 32, No. 2, Mar.–Apr. 1995, pp. 404–410.

[2] Liebeck, R. H., "Design of the Blended Wing Body Subsonic Transport," *Journal of Aircraft*, Vol. 41, No. 1, Jan.–Feb. 2004, pp. 10–25.
doi:10.2514/1.9084

[3] Maxwell, J. C., "On a Particular Case of the Descent of a Heavy Body in

a Resisting Medium," *Cambridge and Dublin Mathematical Journal*, Vol. 9, 1854, pp. 145–148.

[4] Stone, R. W., and Bryant, R. L., "Summary of Results of Tumbling Investigations Made in the Langley 20-Foot Free-Spinning Tunnel on 14 Dynamic Models," NACA RM L8J28, 1948.

[5] Hall, R. M., Biedron, R. T., Ball, D. N., Bogue, D. R., Chung, J., Green, B. E., Grismer, M. J., Brooks, G. P., and Chambers, J. R., "Computational Methods or Stability and Control (COMSAC): The Time Has Come," AIAA Paper 2005-6121, Aug. 2005.

[6] Wooldridge, E. T., *Winged Wonders, The Story of Flying Wings*, 2nd ed., Smithsonian Inst. Press, Washington, D.C., 1985.

[7] Chan, W. M., Rogers, S. E., Nash, S. M., Buning, P. G., and Meakin, R. L., "User's Manual for Chimera Grid Tools, Version 1.6," NASA Ames Research Center, Moffett Field, CA, Sept. 2001.

[8] Buning, P. G., Jespersen, D. C., Pulliam, T. H., Klopfer, G. H., Chan, W. M., Slotnick, J. P., Krist, S. E., and Renze, K. J., "OVERFLOW User's Manual, Version 1.8aa," NASA Langley Research Center, Hampton, VA, Apr. 2003.

[9] Buning, P. G., and Nichols, R., "OVERFLOW2 Training Class," 8th Symposium of Overset Composite Grids and Solution Technology, Houston, TX, Oct. 2006.

[10] Meakin, R. L., "Automatic Off-Body Grid Generation for Domain of Arbitrary Size," AIAA Paper 2001-2536, June 2001.

[11] Meakin, R. L., "Object X-Rays for Cutting Holes in Composite Overset Structured Grids," AIAA Paper 2001-2537, June 2001.

[12] Spalart, P. R., and Allmaras, S. R., "A One-Equation Turbulence Model for Aerodynamic Flows," AIAA Paper 92-0439, Jan. 1992.

[13] Murman, S. M., Chan, W. M., Aftosmis, M. J., and Meakin, R. L., "An Interface for Specifying Rigid-Body Motions for CFD Applications," AIAA Paper 2003-1237, Jan. 2003.

[14] Saephan, S., van Dam, C. P., Fremaux, C. M., and DalBello, T., "Simulations of Flow About Rotating Forebodies at High Angles of Attack," *Journal of Aircraft*, Vol. 41, No. 6, Nov.–Dec. 2004, pp. 1298–1305.
doi:10.2514/1.8984

[15] Mayda, E. A., van Dam, C. P., and Nakafuji, D. Y., "Computational Investigation of Finite Width Microtabs for Aerodynamics Load Control," AIAA Paper 2005-1185, Jan. 2005.

[16] Mayda, E. A., and van Dam, C. P., "Bubble-Induced Unsteadiness on a Wind Turbine Airfoil," *Journal of Solar Energy Engineering*, Vol. 124, No. 4, Nov. 2002, pp. 335–344.

[17] Potsdam, M. A., and Strawn, R. C., "CFD Simulations of Tiltrotor Configurations in Hover," *Journal of the American Helicopter Society*, Vol. 50, No. 1, Jan. 2005, pp. 82–94.

[18] Chao, D. D., and van Dam, C. P., "Computational Aerodynamic Analysis of a Blunt Trailing-Edge Airfoil Modification of the NREL Phase VI Rotor," *Wind Energy*, Vol. 10, No. 6, Nov.–Dec. 2007, pp. 529–550.

[19] Buning, P. G., Gomez, R. J., and Scallion, W. I., "CFD Approaches for Simulation of Wing–Body Stage Separation," AIAA Paper 2004-4838, Aug. 2004.

[20] Gomez, R., Vicker, D., Rogers, S. E., Aftosmis, M. J., Chan, W. M., and Meakin, R. L., "STS-107 Investigation Ascent CFD Support," AIAA Paper 2004-2226, June 2004.

[21] Murman, S. M., Aftosmis, M. J., and Rogers, S. E., "Characterization of Space Shuttle Ascent Debris Using CFD Methods," AIAA Paper 2005-1223, Jan. 2005.

[22] "Debris Transport Analysis," *Columbia Accident Investigation Board Final Report*, Vol. 2, Pt. 8, Oct. 2003, http://caib.nasa.gov/news/report/pdf/vol2/part08.pdf [retrieved Oct. 2006].